

Supporting Information

Eu-MOF and its mixed-matrix membranes as fluorescent sensor for quantitative ratiometric pH and folic acid detection, and visible fingerprint identifying

Yansong Jiang^{1,2†}, Yating Huang^{1†}, Xiangxiang Shi¹, Zijing Lu³, Jiamo Ren¹, Zimo Wang¹, Jianing Xu¹, Yong Fan^{1*}, Li Wang^{1*}

1 *College of Chemistry, Jilin University, Changchun, 130012, Jilin, China*

2 *South China Advanced Institute for Soft Matter Science and Technology, South China University of Technology, Guangzhou, 510640, Guangdong, China*

3 *Hubei Key Laboratory of Mineral Resources Processing and Environment, School of Resources and Environmental Engineering, Wuhan University of Technology, Wuhan, 430072, Hubei, China*

E-mail: lhl222@jlu.edu.cn; lwang99@jlu.edu.cn.

† These authors contributed equally to this work.

Table of Contents

Experimental section	S3
Fig. S1 PXRD patterns of 1 .	S4
Fig. S2 PXRD patterns of 1@PCL and 1@PVDF .	S4
Fig. S3 TGA curve of 1 .	S4
Fig. S4 PXRD patterns of the product after TGA.	S5
Fig. S5 The SEM images of as-synthesized 1 (a) and grind sample (b).	S5
Fig. S6 The cross section SEM and EDS elemental mapping images.	S5
Fig. S7 The effect of ions and anions for FA detection.	S6
Fig. S8 PXRD patterns of 1 in different pH conditions.	S6
Fig. S9 PXRD pattern of 1 after FA detection.	S6
Fig. S10 UV-vis spectrum of analytes.	S7
Fig. S11 The fluorescent spectrum of MMMs.	S7
Fig. S12 The contact angle of MMMs.	S7
Fig. S13 The recycle experiment of 1 and MMMs.	S8
Fig. S14 PXRD patterns of the recycled 1 and MMMs.	S8
Fig. S15 The photographs of MMMs in water or PBS.	S8
Fig. S16 PXRD patterns of 1 , 1@PVDF and 1@PCL after exposed in air for four months.	S9
Table S1 Crystal data and structure refinement for 1 .	S10
Table S2 The selected bond lengths for 1 .	S11
Table S3 The selected bond angles for 1 .	S12
Table S4 The mechanical property of MMMs.	S13
Table S5 The comparison of the detection limit between 1 and other reported chemical sensors for FA detection.	S14
Reference	S14

Experimental section

Material and instruments

All chemical reagents were obtained from commercial sources and used without further purification. Powder X-ray diffraction (XRD) measurements were performed using a SHIMADZU XRD-6000 diffractometer with Cu-K α radiation ($\lambda = 1.5418 \text{ \AA}$). FT-IR spectra were recorded on a Nicolet IS5 spectrometer between 4000 and 400 cm $^{-1}$ using the KBr pellet method. Elemental analyses (C, H and N) were performed using an Elementar Vario EL cube CHNOS elemental analyzer. Thermogravimetric analyses (TGA) were carried out using a PerkinElmer TGA 7 instrument, with a heating rate of 10 °C min $^{-1}$ under air atmosphere. Photoluminescence analyses were performed on an Edinburgh Instrument FLS 920 luminescence spectrometer. UV-vis absorption measurements were carried out on a Shimadzu UV-3100 spectrophotometer. Scanning electron microscopy (SEM) images and Energy-dispersive X-ray spectroscopy (EDS) were obtained with a JEOL JSM-IT500A instrument. The contact angle was determined with a KRÜSS GmbH DSA-25 instrument.

Determination of crystal structure

A suitable single crystal of **1** was carefully picked out under an optical microscope for single crystal XRD analysis. The intensity data was collected on a Bruker P4 diffractometer with graphite-monochromated Mo-K α ($\lambda = 0.71073 \text{ \AA}$) radiation at room temperature. The structure was solved by direct method and refined by full-matrix least-squares on F 2 using OLEX2 equipped with the SHELXTL-2014 crystallographic software packages.[S1-S3] All the hydrogen atoms were placed geometrically and refined in a riding model. All of the non-hydrogen atoms were refined anisotropically. The crystal data and structure refinement for **1** is summarized in Table S1, selected bond lengths and angles are given in Tables S2–S3. CCDC-2081879, contains the supplementary crystallographic data for **1**.

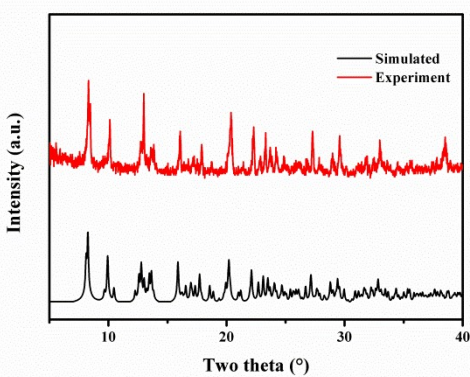


Fig. S1 PXRD patterns of **1**.

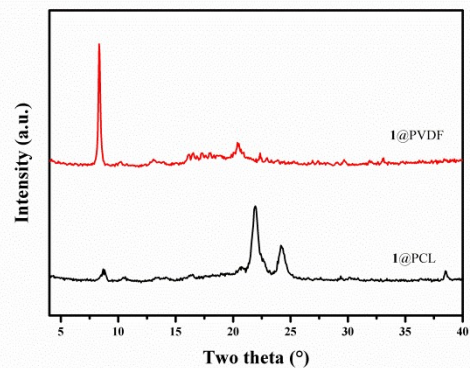


Fig. S2 PXRD patterns of **1@PCL** and **1@PVDF**.

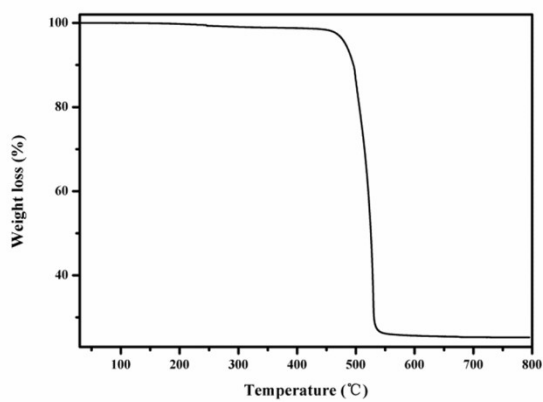


Fig. S3 TGA curve of **1**.

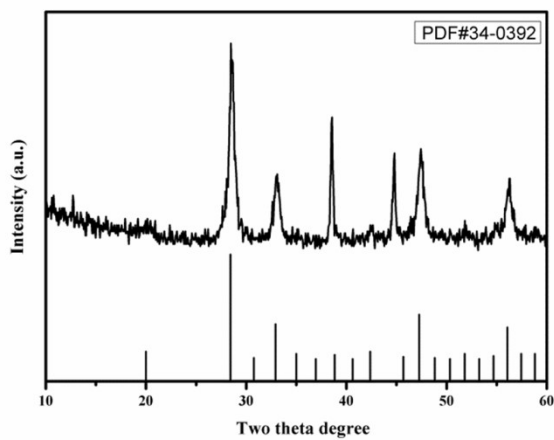


Fig. S4 PXRD patterns of the product after TGA.

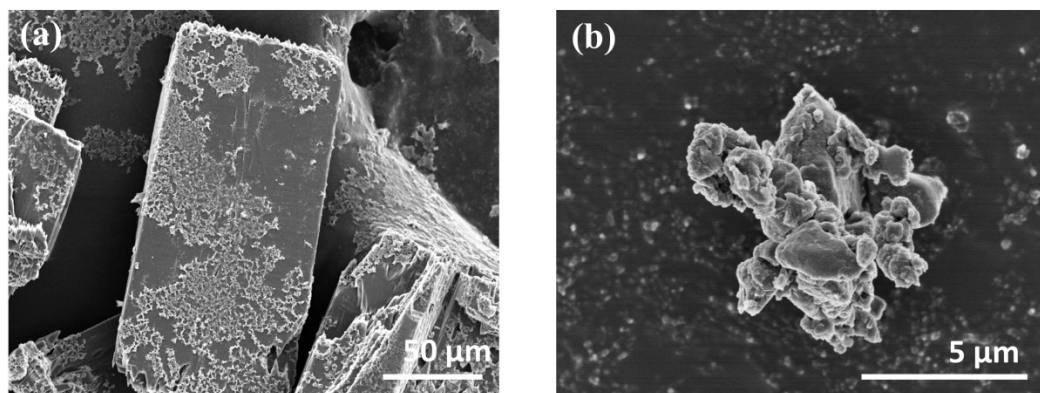


Fig. S5 The SEM images of as-synthesized **1** (a) and grind sample (b).

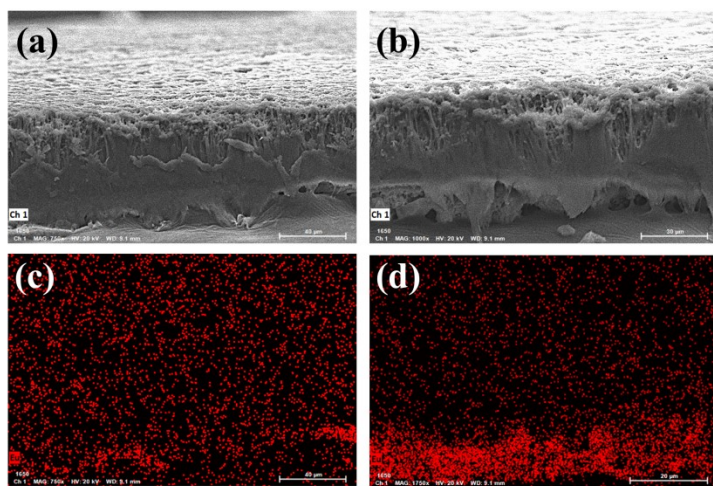


Fig. S6 The cross section SEM images and EDS elemental mapping images (a, c)**1**@PVDF, (b, d)**1**@PCL.

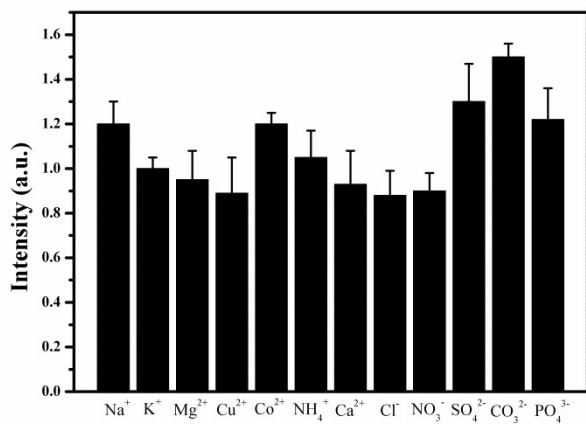


Fig. S7 The effect of ions and anions for FA detection.

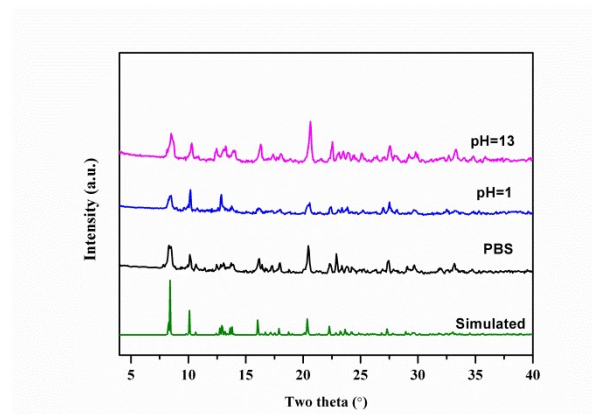


Fig. S8 PXRD patterns of **1** in different pH conditions.

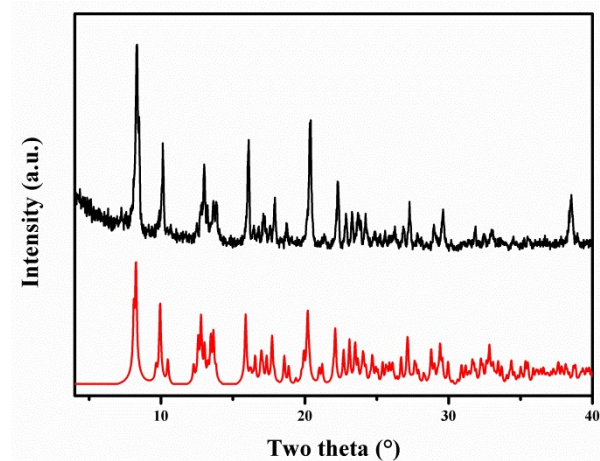


Fig. S9 PXRD pattern of **1** after FA detection.

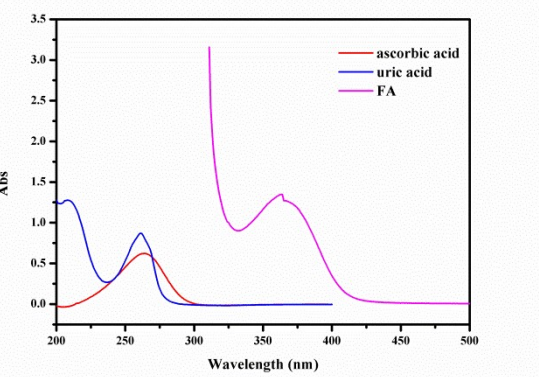


Fig. S10 UV-vis spectrum of analytes.

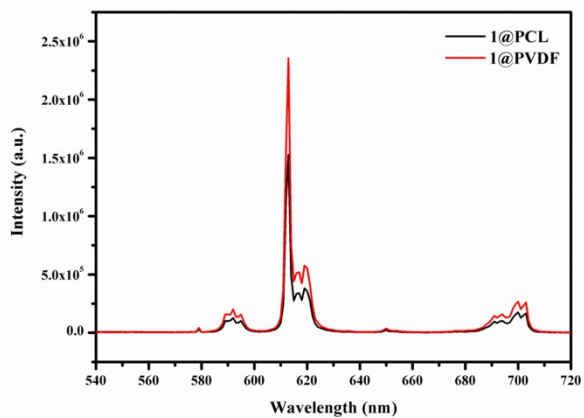


Fig. S11 The fluorescent spectrum of MMMs.

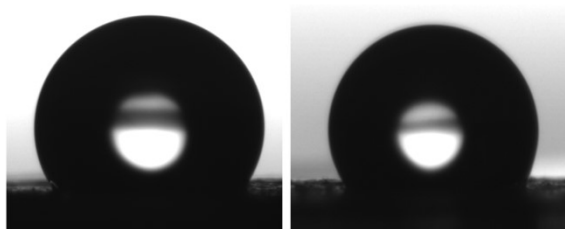


Fig. S12 The contact angle of MMMs. 1@PCL (left: 118.4°) and 1@PVDF (right: 119.7°).

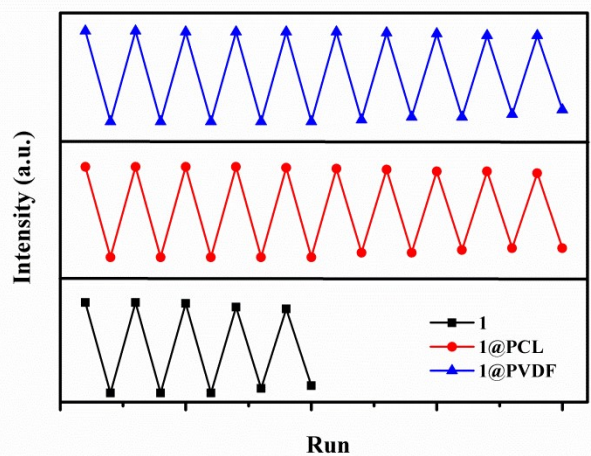


Fig. S13 The recycle experiment of **1** and MMMs.

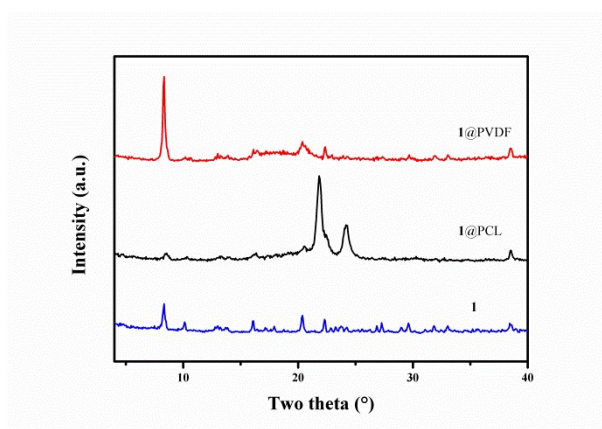


Fig. S14 PXRD patterns of the recycled **1** and MMMs.

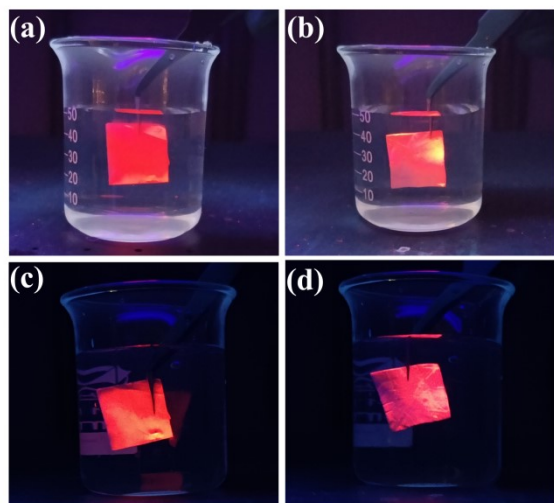


Fig. S15 The photographs of (a) **1**@PVDF in H_2O , (b) **1**@PCL in H_2O , (c) **1**@PVDF in PBS, (d) **1**@PCL in PBS.

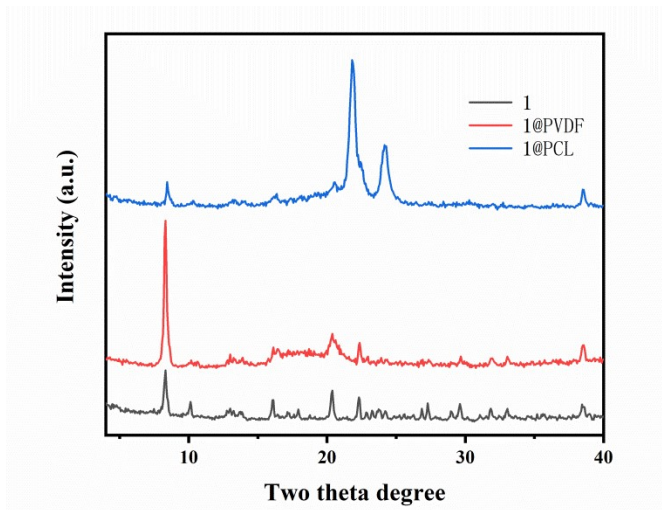


Fig. S16 PXRD patterns of **1**, **1@PVDF** and **1@PCL** after exposed in air for four months.

Table S1 Crystal data and structure refinement for **1**.

Empirical formula	C ₃₄ H ₁₉ EuN ₂ O ₈
Formula weight	735.47
Temperature/K	293(2) K
Crystal system	monoclinic
Space group	P2 ₁ /c
a/Å	11.590(2)
b/Å	16.888(3)
c/Å	14.725(3)
α/°	90.00
β/°	109.92(3)
γ/°	90.00
Volume/Å ³	2709.7(9)
Z	4
ρ _{calc} g/cm ³	1.803
μ/mm ⁻¹	2.377
F(000)	1456.0
Crystal size/mm ³	0.6 × 0.3 × 0.3
Radiation	MoKα ($\lambda = 0.71073$)
2Θ range for data collection/°	6 to 54.86
Index ranges	-14 ≤ h ≤ 14, -21 ≤ k ≤ 21, -16 ≤ l ≤ 19
Reflections collected	23474
Independent reflections	6014 [$R_{int} = 0.0623$, $R_{sigma} = 0.0541$]
Data/restraints/parameters	6014/0/406
Goodness-of-fit on F ²	1.031
Final R indexes [I>=2σ (I)]	$R_I = 0.0351$, $wR_2 = 0.0630$
Final R indexes [all data]	$R_I = 0.0504$, $wR_2 = 0.0689$
Largest diff. peak/hole / e Å ⁻³	0.62/-1.75

Table S2 The selected bond lengths for **1**.

Atom	Atom	Length/ \AA
Eu1	Eu1 ¹	4.2067(7)
Eu1	O1	2.450(3)
Eu1	O2	2.442(3)
Eu1	O8 ²	2.356(3)
Eu1	O4 ³	2.325(3)
Eu1	O7 ⁴	2.303(3)
Eu1	O3 ⁵	2.369(3)
Eu1	N1	2.614(4)
Eu1	N2	2.543(3)
Eu1	C8	2.812(4)
Eu1	C22 ²	3.140(4)
O1	C8	1.257(5)
O2	C8	1.271(5)
O8	Eu1 ⁶	2.356(3)
O8	C22	1.243(5)
O4	Eu1 ⁷	2.325(3)
O4	C7	1.260(5)
O7	Eu1 ⁸	2.303(3)
O7	C22	1.263(5)
O3	Eu1 ⁹	2.369(3)

¹1-X,1-Y,2-Z; ²1+X,1/2-Y,1/2+Z; ³1-X,1/2+Y,3/2-Z; ⁴-X,1/2+Y,3/2-Z; ⁵+X,1/2-Y,1/2+Z; ⁶-1+X,1/2-Y,-1/2+Z; ⁷1-X,-1/2+Y,3/2-Z; ⁸-X,-1/2+Y,3/2-Z; ⁹+X,1/2-Y,-1/2+Z

Table S3 The selected bond angles for **1**.

Atom	Atom	Atom	Angle/ [°]	Atom	Atom	Atom	Angle/ [°]
O1	Eu1	N1	76.76(10)	O7 ⁵	Eu1	O8 ²	125.84(11)
O1	Eu1	N2	89.96(11)	O7 ⁵	Eu1	O4 ⁴	74.27(10)
O1	Eu1	C8	26.50(10)	O7 ⁵	Eu1	O3 ³	79.98(10)
O1	Eu1	C22 ²	164.21(10)	O7 ⁵	Eu1	N1	144.01(11)
O2	Eu1	O1	53.32(9)	O7 ⁵	Eu1	N2	146.89(11)
O2	Eu1	N1	112.59(10)	O7 ⁵	Eu1	C8	77.88(11)
O2	Eu1	N2	73.46(11)	O7 ⁵	Eu1	C22 ²	106.31(11)
O2	Eu1	C8	26.84(10)	O3 ³	Eu1	O1	129.73(10)
O2	Eu1	C22 ²	140.34(10)	O3 ³	Eu1	O2	76.70(9)
O8 ²	Eu1	O1	145.82(10)	O3 ³	Eu1	N1	135.46(10)
O8 ²	Eu1	O2	141.96(10)	O3 ³	Eu1	N2	79.71(10)
O8 ²	Eu1	O3 ³	78.00(10)	O3 ³	Eu1	C8	103.31(11)
O8 ²	Eu1	N1	69.07(11)	O3 ³	Eu1	C22 ²	65.32(10)
O8 ²	Eu1	N2	74.43(11)	N1	Eu1	C8	95.50(11)
O8 ²	Eu1	C8	155.50(11)	N1	Eu1	C22 ²	88.51(11)
O8 ²	Eu1	C22 ²	20.43(10)	N2	Eu1	N1	63.40(11)
O4 ⁴	Eu1	O1	89.74(10)	N2	Eu1	C8	81.70(11)
O4 ⁴	Eu1	O2	135.10(10)	N2	Eu1	C22 ²	88.43(11)
O4 ⁴	Eu1	O8 ²	82.90(11)	O4 ⁴	Eu1	C8	112.60(11)
O4 ⁴	Eu1	O3 ³	129.36(10)	O4 ⁴	Eu1	C22 ²	81.10(11)
O4 ⁴	Eu1	N1	76.00(10)	O7 ⁵	Eu1	O1	83.25(11)
O4 ⁴	Eu1	N2	138.29(11)	O7 ⁵	Eu1	O2	76.58(10)

¹1-X,1-Y,2-Z; ²1+X,1/2-Y,1/2+Z; ³+X,1/2-Y,1/2+Z; ⁴1-X,1/2+Y,3/2-Z; ⁵-X,1/2+Y,3/2-Z; ⁶-1+X,1/2-Y,-1/2+Z; ⁷1-X,-1/2+Y,3/2-Z; ⁸-X,-1/2+Y,3/2-Z; ⁹+X,1/2-Y,-1/2+Z

Table S4 The mechanical property of MMMs.

	F m (N)	σ_m (MPa)	ϵ_m (%)	E t (MPa)	ϵ_b (%)	F b (N)	σ_b (MPa)	U b (mJ)
1@PCL	4.10	1.02	48	7.64	68	1.30	0.325	20.2
1@PVDF	6.25	10.4	6.1	408	140	-0.0150	-0.0250	40.8

Table S5 The comparison of the detection limit between **1** and other reported chemical sensors for FA detection.

Materials	Detection limit (M)	Reference
Y ₂ O ₃ :Eu	0.083 × 10 ⁻⁶	S4
CdTe	0.095 × 10 ⁻⁶	S5
Carbon dots	1.2 × 10 ⁻⁶	S6
ZnS: Mn or Cu	1.1 × 10 ⁻⁵	S7
CdInS ₂ QDs	8 × 10 ⁻⁵	S8
1,10-phenanthroline-Tb(III)-Ag NPs	0.21 × 10 ⁻⁶	S9
MoS ₂ QDs	0.1 × 10 ⁻³	S10

Reference

- [S1] O.V. Dolomanov, L.J. Bourhis, R.J. Gildea, J.A.K. Howard, H. Puschmann, OLEX2: a complete structure solution, refinement and analysis program, *Journal of Applied Crystallography*, 2009, 42, 339–341.
- [S2] G. Sheldrick, Crystal structure refinement with SHELXL, *Acta Crystallographica Section C*, 2015, 71, 3-8.
- [S3] G. Sheldrick, A short history of SHELX, *Acta Crystallographica Section A*, 2008, 64, 112–122.
- [S4] F. Gudarzy, A.B. Moghaddam, S. Mozaffari, *et al.* A lanthanide nanoparticle-based luminescent probe for folic acid. *Microchim Acta* 2013, 180, 1257–1262.
- [S5] P. Nagaraja, R.A. Vasantha. Spectrophotometric determination of folic acid in pharmaceutical preparations by coupling reactions with iminodibenzyl or 3-aminophenol or sodium molybdate–pyrocatechol. *Anal Biochem* 2002, 307, 316–321.
- [S6] S.Y. Liu, J.J. Hu, X.G. Su Detection of ascorbic acid and folic acid based on water-soluble CuInS₂ quantum dots. *Analyst* 2012, 137, 4598–4604.
- [S7] B. Zeng, F. Zhao. Single-walled carbon nanotube-ionic liquid paste electrode for the sensitive voltammetric determination of folic acid. *Sens Actuat B* 2008, 134, 895–901.
- [S8] S.Q. Han, X.X. Chen. Copper nanoclusters-enhanced chemiluminescence for folic acid and nitrite detection. *Spectrochim Acta A* 2019, 210, 315–320.
- [S9] Y. Ganjkhelanlou, M. Kazemzad, F. Alikhani Hessari. Chromaticity dependence on Eu concentration in Y₂O₃:Eu nanopowders. *Nano: Brief Report Rev* 2010, 5, 111–116.
- [S10] Y. Peng, W. Dong, L. Wan, *et al.* Determination of folic acid via its quenching effect on the fluorescence of MoS₂ quantum dots. *Microchim Acta* 2019, 186, 605.